Earthquakes and Structures, *Vol. 7, No. 5 (2014) 797-815*
DOI: http://dx.doi.org/10.12989/eas.2014.7.5.797

Experimental and analytical assessment of SRF and aramid composites in retrofitting RC columns

Hoang V. Dang[1], Myoungsu Shin[2], Sang Whan Han[3] and Kihak Lee[*1]

[1]*Department of Architectural Engineering, Sejong University, 98 Gunja-dong, Gwangjin-gu, Seoul 143-747, Republic of Korea*
[2]*School of Urban and Environmental Engineering, Ulsan National Institute of Science and Technology, Unist-gil 50, Ulsan 689-798, Republic of Korea*
[3]*Department of Architectural Engineering, Hanyang University, Wangsipli-ro 222, Seongdong-gu, Seoul 133-791, Republic of Korea*

(Received April 25, 2014, Revised August 6, 2014, Accepted August 16, 2014)

Abstract. This research aimed to investigate retrofitting methods for damaged RC columns with SRF (Super Reinforced with Flexibility) and aramid composites and their impacts on the seismic responses. In the first stage, two original (undamaged) column specimens, designed to have a flexural- or shear-controlled failure mechanism, were tested under quasi-static lateral cyclic and constant axial loads to failure. Afterwards, the damaged column specimens were retrofitted, utilizing SRF composites and aramid rods for the flexural-controlled specimen and only SRF composites for the shear-controlled specimen. In the second stage, the retrofitted column specimens were tested again under the same conditions as the first stage. The hysteretic responses such as strength, ductility and energy dissipation were discussed and compared to clarify the specific effects of each retrofitting material on the seismic performances. Generally, SRF composites contributed greatly to the ductility of the specimens, especially for the shear-controlled specimen before retrofitting, in which twice the deformation capacity was obtained in the retrofitted specimen. The shear-controlled specimen also experienced a flexural failure mechanism after retrofitting. In addition, aramid rods moderately fortified the specimen in terms of the maximum shear strength. The maximum strength of the aramid-retrofitted specimen was 12% higher than the specimen without aramid rods. In addition, an analytical modeling of the undamaged specimens was conducted using Response-2000 and Zeus Nonlinear in order to further validate the experimental results.

Keywords: SRF composites; aramid rods; hysteretic behavior; displacement ductility; seismic retrofit

1. Introduction

Recently, many old existing concrete structures were intensively devastated during severe earthquakes, resulting in heavy loss of human lives and properties. Due to a common deficiency (i.e. lack of transverse reinforcement or confinement), columns in those structures usually experienced shear failure, where weak column-strong beam conditions existed, which led to

*Corresponding author, Professor, kihaklee@sejong.ac.kr

http://www.techno-press.org/?journal=eas&subpage=7 ISSN: 2092-7614 (Print), 2092-7622 (Online)

significant structural damages or complete collapses of the whole structures. Taking that into consideration, new structures, located in high seismic regions, are stringently designed in accordance with stricter requirements in many building codes. Also, the strengthening of existing concrete structures with extra reinforcement has also been regarded as effective and economical ways to reduce damages.

Analytical and experimental studies of various composite materials have been undertaken to investigate their reinforcing effects on existing concrete structures. Choi *et al*. (2014) presented a multi-objective seismic retrofit method using fiber-reinforced polymer (FRP) jackets in shear-critical reinforced concrete (RC) frames. Non-dominated sorting genetic algorithm-II (NSGA-II) was used to optimize the cost and seismic performance of the retrofitting material. This research also considered the shear failure of columns. Carbon fiber reinforced polymer (CFRP) has also been a popular solution for strengthening existing structures. Le *et al*. (2010) presented both experimental study and analytical modeling of RC beam-column joints strengthened using CFRP composites. Colomb *et al*. (2008) tested their CFRP-retrofitted short RC columns to evaluate the contribution of CFRP to the mechanical and energetic performance, and its effects on the cracking pattern. Dai *et al*. (2012) investigated the seismic response of square RC columns retrofitted with polyethylene terephthalate (PET)-FRP, which has a higher tensile capacity than conventional ones. The results showed that PET-FRP significantly improved the displacement ductility of RC columns and prevented them from rupturing.

Many stiff and strong FRP strengthening materials, commonly plated or wrapped using adhesive, have fractured or peeled under high stresses, resulting in damage to the attached concrete surfaces. Super Reinforced with Flexibility (SRF) material, developed by Dr. Shunuchi Igarashi, shares characteristics such as toughness, durability, heat-resistance with other conventional FRPs, and is mainly different in its high flexibility.

Kim *et al*. (2012) carried out experiments applying the SRF strengthening method. The flexibility of the SRF material prevented it from being peeled off the concrete surface and subsequent brittle failure. In addition, previous studies proved that the SRF strengthening method significantly enhanced RC structures in terms of ductility by increasing their deformation capacities in both vertical and lateral directions. However, in comparison with conventional FRP strengthening methods, SRF strengthening methods showed less than expected impacts in enhancing the initial stiffness and ultimate strength of RC members.

The current research focused on damaged RC columns and their seismic behaviors after being strengthened with SRF and/or aramid rods (one type of FRP). Both flexure-controlled and shear-controlled column specimens were considered as the subject of retrofit.

In the first stage, initial (undamaged) column specimens were tested under lateral cyclic and constant axial loads to failure. The damaged column specimens were then retrofitted, utilizing SRF composites and/or aramid rods. In the second stage, the retrofitted column specimens were tested under the same conditions as the first stage. The hysteretic responses such as strength, ductility and energy dissipations were discussed and compared to clarify the specific effects of each retrofitting material on the seismic behaviors. Also, an analytical modeling of the primary undamaged specimens was conducted to further validate the experimental results. The purpose of this research is to investigate the effects of SRF and aramid rods in terms of (1) their abilities to recover and enhance the seismic performance of the damaged specimens and (2) the level of such impacts depending on RC column failure mechanisms. In addition, the combined use of both internal and external retrofitting methods was evaluated in retrofitting RC columns.

2. Experimental program and retrofitting procedure

2.1 Experimental program

2.1.1 Design of column specimens

Table 1 presents the mechanical properties of the materials used in this study. Longitudinal and transverse reinforcements used for the column specimens were D19 (19.05 mm diameter) and D10 (9.525 mm diameter), respectively. Three samples of each reinforcing bar (D19 for the main bars and D10 for the stirrups) were tested under tension, and of the measured stress-strain relationships are provided in Fig. 1.

The column specimens had all design details in common except the varying spacing of the stirrups. Transverse reinforcement is generally considered to serve three main functions, namely, confining the concrete core, restraining the buckling of longitudinal bars, and avoiding shear failure. Hence, the variation of the stirrup spacing in the column specimens can lead to large differences regarding the three actions mentioned above. More specifically, the wider the spacing between the stirrups is, the less confinement is provided to the core concrete; the longitudinal bars also become poorly supported and unable to avoid buckling, resulting in non-ductile behavior and sudden brittle failure of the columns. In this study, two different stirrup's spacing were considered in order to deliberately induce two different failure modes each: flexure-controlled (FC) and shear-controlled (SC).

The specimens were designed similar to those in Han and Jee (2005). All test specimens had the same rectangular section of 300 mm × 300 mm. Eight longitudinal bars were evenly distributed around the rectangular perimeter, in which the clear cover was 26.67 mm. The spacing of transverse reinforcement was designed to be 300 mm for the SC failure-mode specimen, while it was 100 mm for the FC failure-mode specimen. The specimens were tested subjected to lateral loading under a constant compressive axial load (10% of the column capacity equal to $0.1f_c'A_g$; where f_c' is the compressive strength of the concrete; A_g is the gross sectional area of the column). The test specimens were 900 mm in height. Each specimen represented an approximately 2/3-scale model of the lower half of the prototype column; the height of the prototype columns is 2700 mm. The prototype column is considered to develop an inflection point at mid-height, when subjected to lateral loading. More design details on the test specimens are given in Table 2.

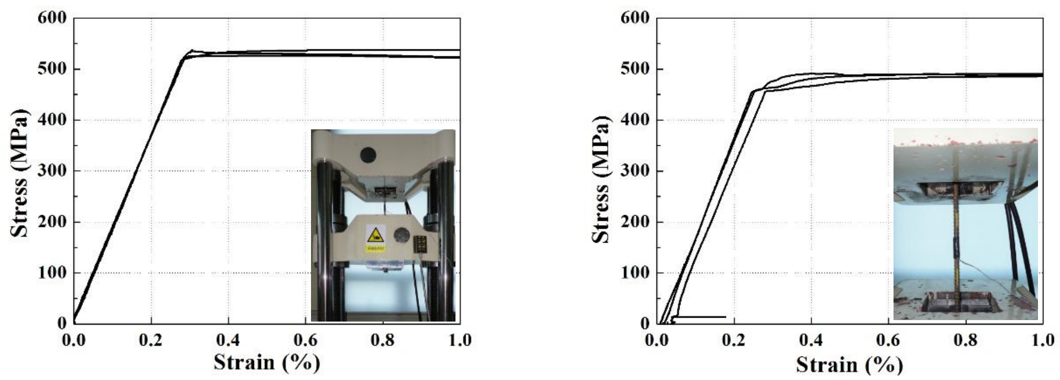

(a) Transverse reinforcement (D10) (b) Longitudinal reinforcement (D19)

Fig. 1 Stress-strain relationships of steel reinforcements

Table 1 Mechanical properties of concrete and steel reinforcements

Mechanical properties	Concrete compressive strength	Longitudinal reinf. (D19)		Transverse reinf. (D10)	
		Tensile strength	Young's modulus	Tensile strength	Young's modulus
Design value	27.0	400.0	200,000	400.0	200,000
Measured value	32.6	484.7	190,870	528.3	183,697

*Unit: MPa

Table 2 Design details of the test specimens

Specimen names	FC (Flexural-Controlled)	SC (Shear-Controlled)
Section dimension	300x300 mm	300x300 mm
Clear cover	26.67 mm	26.67 mm
Longitudinal reinforcement	8-D19	8-D19
Volumetric longitudinal reinforcement ratio ρ_L	2.55%	2.55%
Stirrup spacing	D10@100 mm	D10@300 mm
Volumetric transverse reinforcement ratio ρ_S	1.20%	0.40%
Axial load (ratio of axial force capacity)	243 kN ($0.1f_c'A_g$)	243 kN ($0.1f_c'A_g$)
Specimen height	900 mm	900 mm
Aspect ratio (Height/Section dimension)	3.0	3.0

2.1.2 Loading setup and instrumentation

Fig. 3 presents an aerial picture and a schematic illustration for the test setup. The loading system consisted of a horizontal hydraulic actuator of a 500-kN capacity for applying lateral loading and a vertical actuator of a 300-kN capacity for axial compressive loading. Steel reaction frames and a concrete reaction wall formed the reaction force system for the actuators. The solid concrete foundation with the specimen attached was firmly anchored to the ground to avoid the specimen sliding or overturning during the test. Because the axial load actuator remained in the same position during the test while the column specimen laterally deflected, a sliding device was provided between the top of the column and the actuator.

With respect to experimental instrumentation, electrical-resistance strain gauges and linear variable differential transformers (LVDTs) were used in the tests. Each of the four longitudinal bars were attached a strain gauge at the same height position to form a layer of gauges. In each specimen, five layers were distributed at different height levels from the bottom to top of the specimen. Each stirrup was attached with three strain gauges on the perimeter.

Cyclic lateral displacements were imposed at the top of the column with steadily increasing demand level. Quasi-static displacement-controlled reversed cyclic loading was applied. Three consecutive cycles were applied for each displacement level from 0.25% to 1% drift ratio, while from 1.5% drift ratio, only two cycles were applied. The loading history is shown in Fig. 4. Similar operations carried out by many researchers have proven the efficiency of this procedure for evaluating the seismic performance of RC members, as well as offering information for the development and calibration of numerical models. The stiffness and strength deterioration of the test specimen was investigated through repetitive cycles for each displacement level.

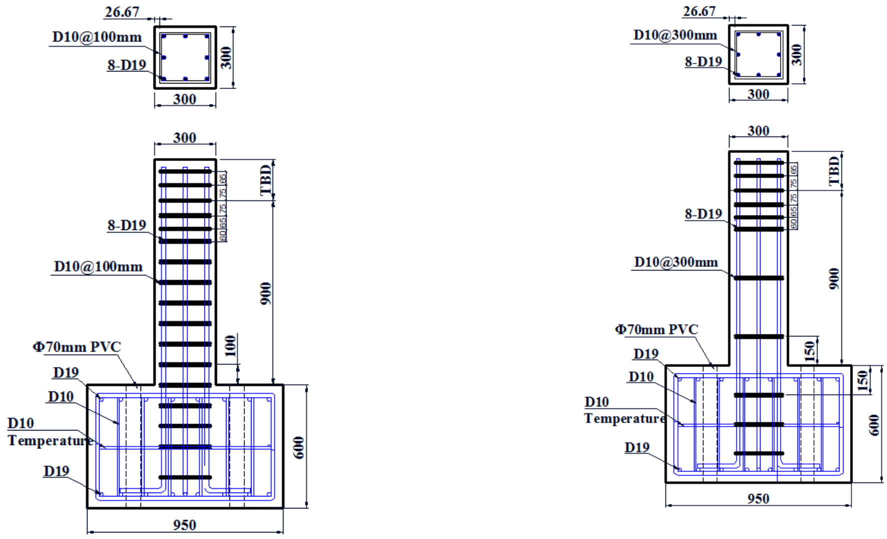

(a) Specimen FC (b) Specimen SC

Fig. 2 Undamaged specimen dimensions and reinforcement details

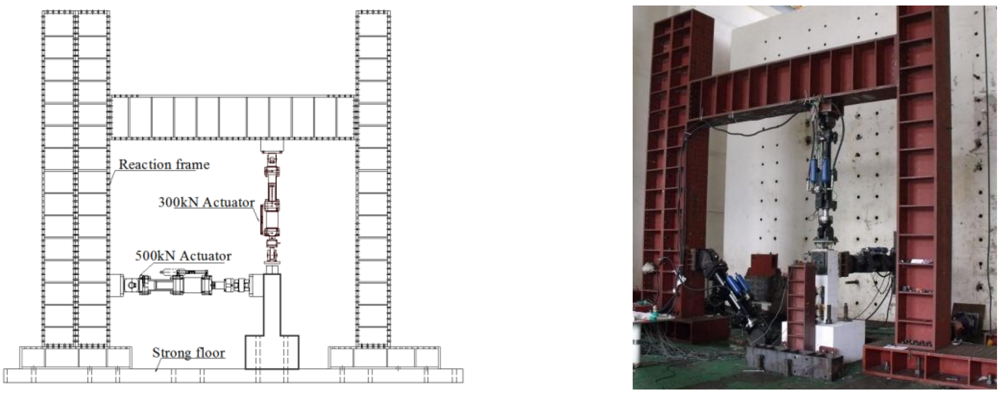

Fig. 3 Test setup and instrumentation

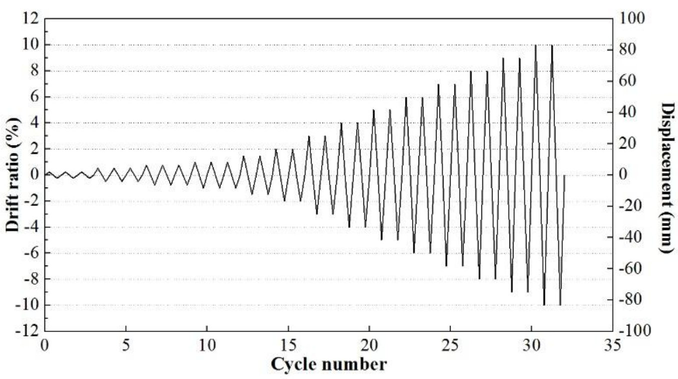

Fig. 4 Loading history

2.2 Retrofitting procedure

In this study, SRF composites and aramid fiber rods were two among many potential retrofitting materials that have been adopted to strengthen the damaged column specimens. Fig. 5 presents the retrofitting materials used for the tests. As mentioned above, SRF materials were expected to have a significant effect in improving the ductility, as well as in maintaining the axial load-carrying capacity of the column specimen. Therefore, both the FC and SC specimens were retrofitted with SRF materials in order to investigate its influence on those with the two different failure modes. In addition, aramid fiber rods, which have a high ultimate tensile strength and elasticity modulus, were used as longitudinal bars to retrofit the FC specimen. The specific details of the retrofitting methods for the FC and SC specimens are presented in Table 3. It is noted that, the retrofitting method for the FC specimen differed from that for the SC specimen only by the addition of the aramid fiber rods. The retrofitted “new” specimens were designated as Specimens RFC and RSC corresponding to the original FC and SC specimens, respectively. The width and thickness of SRF sheets used in the tests are 100 mm and 2.5 mm, respectively. Table 4 shows the mechanical properties of the aramid rod and polyester sheet.

Polyurethane adhesive was used to apply the SRF sheets on the specimens. The SRF retrofitting process consisted of the following steps. First, all the side surfaces of the column were exposed to evenly apply the polyurethane adhesive. Then, the SRF sheets were tightly wrapped around the column with a tension force, from the bottom to the top of the specimen, so that it would not get loose during the process. The sheets were then anchored using adhesive and taped to finish the process.

For the RFC specimen, eight aramid rods were attached directly to the original longitudinal bars. In order to get aramid rods anchored into the foundation below the column, 30 mm holes were drilled in the foundation at positions adjacent to the original longitudinal bars. Each aramid rod was put in the hole and then was tied to the longitudinal bars using iron wires.

In the second stage of the experimental program, the column specimens damaged in the first stage were rehabilitated in preparation for the next tests. This rehabilitation was simply implemented by the following steps. First, concrete debris from the cracked covers of the column specimens was clearly removed to expose the column longitudinal bars. Second, strain gauges were attached to the longitudinal bars. Then, each of eight aramid rods was installed along each longitudinal bar and attached using iron wires. Finally, all surfaces of the column specimen were covered with cement mortar to form the original column dimensions. Afterwards, the specimens were cured for 28 days before being wrapped with SRF sheets using Polyurethane adhesive. Fig. 6 shows the retrofitting procedures for the column specimens.

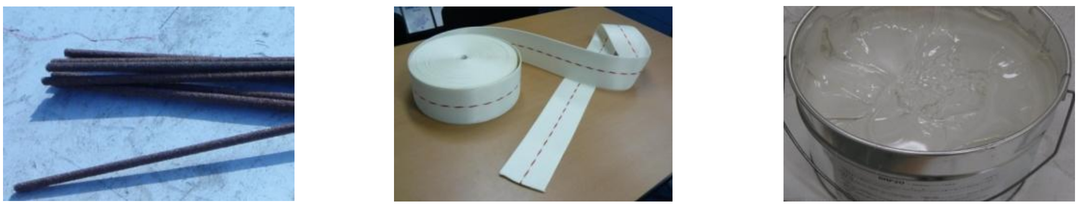

(a) Aramid fiber rods (b) Polyester sheet (c) Polyurethane adhesive

Fig. 5 Aramid fiber rods and SRF materials

(a) Remove the debris from the crack cover

(b) Attach strain gauges

(c) Attach Aramid rods to the l ongitudinal reinforcements

(d) Cover the specimen wit h cement-mortar

(e) Cure the covered specimen for 28 days

(f) Wrap the specimen with SR F composite sheet

Fig. 6 Aramid rod and SRF sheet installations in the column specimens

Table 3 Methods for retrofitting the test specimens

Methods	Specimen FC	Specimen SC
SRF sheets	✓	✓
Aramid fiber rods	✓	-
Name of retrofitted Specimen	**RFC** (Retrofitted-FC)	**RSC** (Retrofitted-SC)

Table 4 Mechanical properties of Aramid fiber-reinforced polymer rod and Polyester sheet

	Ultimate tensile strength	Elasticity modulus (MPa)	Fracture strain (%)
Aramid rod	1,400 (MPa)	76,100	1.83
Polyester sheet	1,000 (N/mm)	4,000	10.0

3. Experimental results and evaluations

In this section, the experimental results, comprised of hysteretic curves, ductility and energy dissipation are presented and verified. The general impacts of retrofitting with SRF and aramid rods are obtained and discussed, and specific influences that were observed are interpreted in comparisons between FC and SC specimens.

3.1 Hysteretic performance and ductility of specimens

Fig. 7 presents the hysteretic curves of both primary FC and SC specimens and the retrofitted versions under the same loading conditions. All column specimens exhibited the first yielding at the drift ratio of about 0.75%. The difference between the FC and SC specimens was quite clear; the FC was dominated by the flexural critical failure mechanism, and the SC by shear critical, respectively. Both FC and SC specimens reached similar maximum applied loads (155 kN for the FC and 149 kN for the SC specimen). At the same time, the FC specimen reached a drift ratio of 2% while SC reached 1.5%. Afterwards, the strength of Specimen FC gradually decreased till it ruptured at a maximum deformation of 6%, while the SC specimen suddenly dropped and promptly failed at the next drift ratio of 3%. In addition, crack propagation of the FC and SC specimens are showed in Fig. 8 (a)-(b). It can be seen that, at failure, the FC exhibited short major cracks at the plastic hinging region started from the column-to-footing surface while long cracks occurred in the inclined plane along the SC specimen. At the same drift ratio of 3%, the SC specimen was severely damaged with more cracks than the FC specimens.

Visually, the RSC specimen hysteretic curve showed that it was extensively enhanced from the original specimen, while the effect seemed to be less significant in the case of the RFC specimen. Though slight differences could be found between the RFC and RSC, the more fundamental structural properties were calculated to verified specific impacts of the retrofitting methods on each specimen. Table 5 presents the measured and calculated strengths, displacements and ductility of all specimens. In addition, nominal shear strength of specimens are calculated according to ACI 318-11, only contributions of concrete V_c and transverse reinforcements V_s are considered. Nominal flexural strength of the FC and SC were determined by using the interaction diagram of the column. For the retrofitted RFC and RSC specimens, due to the concrete cracking and reinforcement yielding, shear strength is predicted from the shear strength at failure of the initial specimen and contributions of retrofitting materials. Contribution of SRF sheet V_f is considered for both RFC and RSC specimens and given by the following formula adopted from Ghobarah and Galal (2004),

$$V_f = 0.95(2t_f)(\varepsilon_{fe}E_f)d_f \tag{1}$$

where, t_f is the thickness, ε_{fe} is the design strain and E_f is the Young Modulus of SRF sheet; d_f is the depth of SRF sheet in the direction of load. Contribution of Aramid fiber rods was calculated using ACI 440.1R-06. Due to lower strength and stiffness of aramid rod in the transverse direction, its distribution was neglected, however, the contribution of concrete Vc when using aramid rods as main reinforcement was recalculated.

Shear strengths estimated by ACI 318-11 of specimens FC and SC is 288.7 kN and 156.2 kN, respectively. The maximum shear capacity of FC and SC specimens are similar, which are 155 kN and 149 kN, respectively. The estimated shear strength is quite precise in case of SC specimens (4.6% error). It is noted that, at drift ratio of 1.5%, both FC and SC specimen have yet to suffer any major crack, only hairline cracks could be found. After that, major cracks occurred in specimens as they reached their shear capacity. The impact of transverse reinforcement, which is prevent specimen from brittle failure, became effective right after major cracks occurred in specimens. SC specimen, due to less transverse bars, promptly failed at the next drift ratio of 3%. In FC specimen, narrow transverse bars' spacing led to gradual strength drop instead of increasing shear strength as afore predicted. Estimated shear strengths of RFC and RSC specimens are 123.3 kN and 97 kN, which are closed to experimental results, 137 kN and

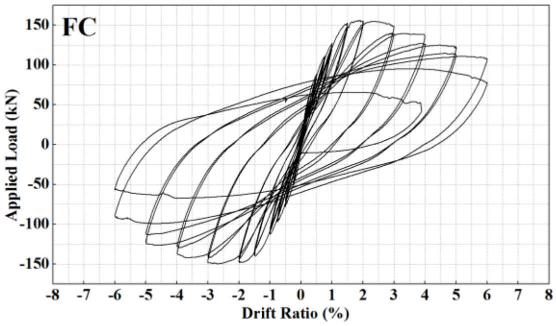

(a) Specimen FC (primary)

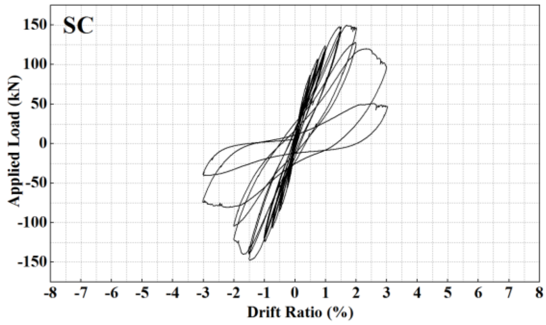

(b) Specimen SC (primary)

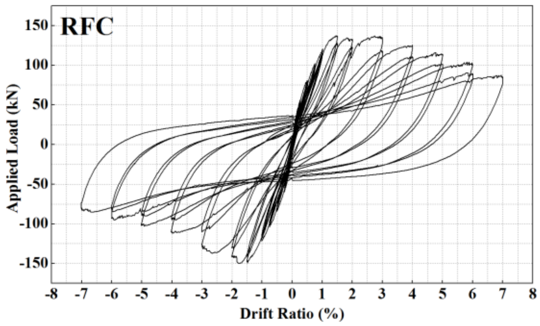

(c) Specimen RFC (retrofitted)

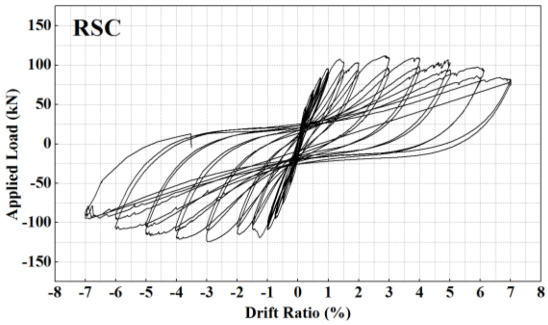

(d) Specimen RSC (retrofitted)

Fig. 7 Hysteretic load-drift curves of the initial and retrofitted column specimens

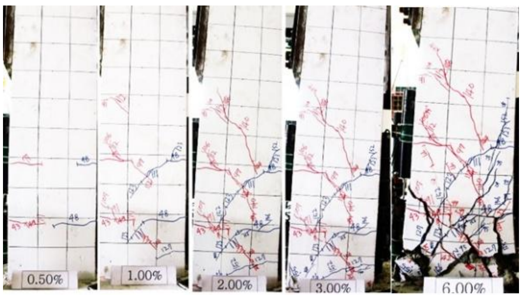

(a) Specimen FC (Failure at 6%)

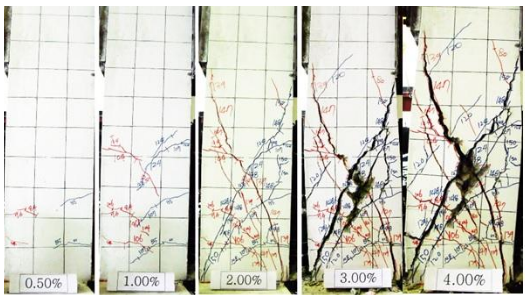

(b) Specimen SC (Failure at 3%)

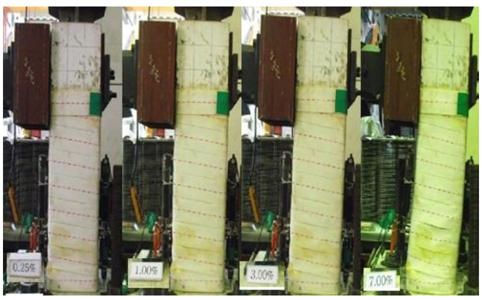
(c) Specimen RFC (Failure at 7%)

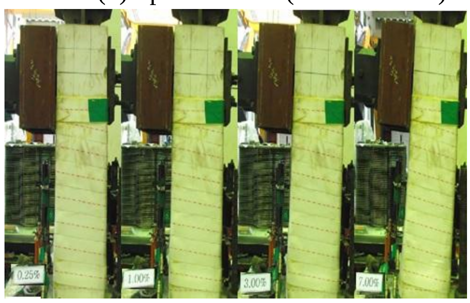
(d) Specimen RSC (Failure at 7%)

Fig. 8 Cracks propagation with each drift level in the specimens

Table 5 Measured and calculated strengths, displacements and ductility of specimens

Specimens	FC	RFC	SC	RSC
Yield strength (kN)	106	102	105	83
Yield displacement – drift	6.5 mm	6.8 mm	6.3 mm	6.6 mm
δ_y	(~ 0.75%)	(~ 0.75%)	(~ 0.75%)	(~ 0.75%)
Max. applied load (kN)	155	137	149	111
Nominal shear strength (kN)	288.7	123.3	156.2	97
Nominal flexural strength (kNm)	121	-	121	-
Drift at max. applied load	2%	1.5%	1.5%	3%
Ultimate displacement – drift	44 mm	54 mm	22.5 mm	63 mm
δ_u	(~ 5%)	(~ 6%)	(~ 2.5%)	(~ 7%)
Ductility δ_u / δ_y	6.7	7.9	3.5	9.5
Ratio of ductility increase	-	1.18*	-	2.71

* 7.9/6.7 = 1.18

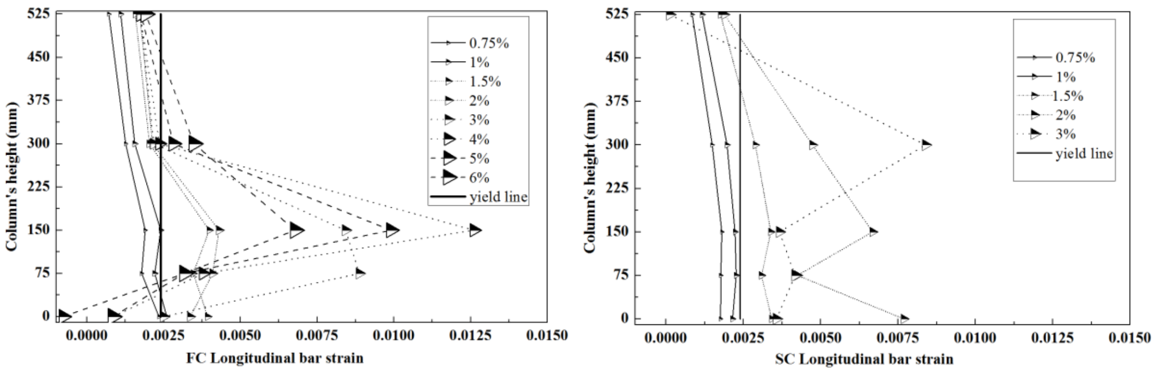

(a) Specimen FC's longitudinal bar strain (b) Specimen SC's longitudinal bar strain

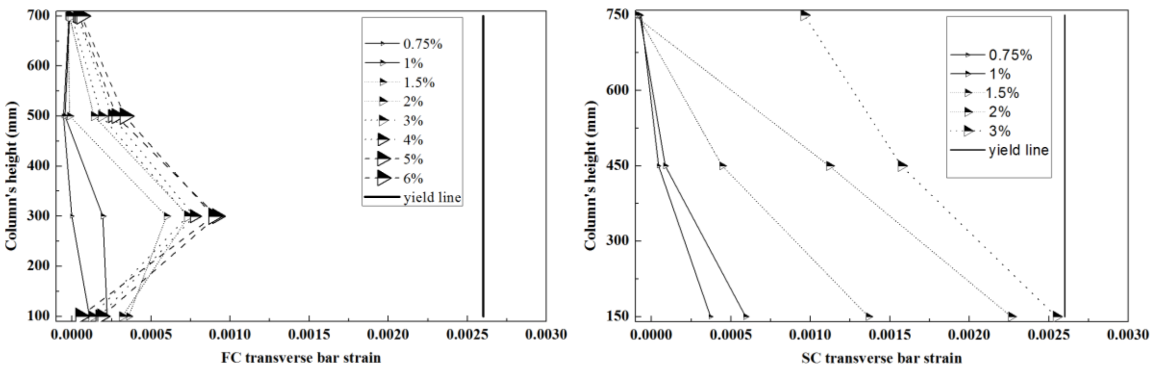

(c) Specimen FC's transverse bar strain (b) Specimen SC's transverse bar strain

Fig. 9 Longitudinal and transverse bar strain distribution

111 kN with error of 10% and 12%, respectively.

The ultimate displacements were conventionally calculated from the point of 20% strength drop from the maximum applied loads. Then, the ductility of the specimen was calculated by dividing the ultimate displacement by the yield displacement. First yielding point is determined based on method proposed by

Park (1989) as the peak of the cycle in which the strength is equal or lower than three-quarters of the maximum strength.

Firstly, it can be seen that both FC and SC specimens behaved more ductile after the retrofit. Ductility of the RFC increased by 18% and RSC increased by 171% compared to the FC and SC, respectively. The results confirmed that the SFR material significantly fortified the columns in term of their ductility. Moreover, the level of effect seemed to depend on the failure mechanism of the original specimen. The shear failure specimen was much more likely to be strongly enhanced than the flexural failure specimen. The RSC specimen even exceeded the RFC in ductile behavior, nearly 20% in terms of ductility.

Secondly, after retrofit neither column specimen could sustain the same maximum load that it had sustained in the first stage. The load-bearing capacity of the specimens decreased by 11.6% for the RFC (137 kN) and 25.5% for the RSC (111 kN) compared to their original FC (155 kN) and SC (149 kN) specimens, respectively. As noted earlier, the RFC specimen, which was retrofitted with extra aramid fiber rods, restored more column strength than the RSC specimen without aramid rods.

Longitudinal and transverse reinforcements strain distribution of FC and SC specimens are presented in Fig. 9. It is noted that yield strain of longitudinal and transverse reinforcement are 0.0024 and 0.0026, respectively, and were illustrated by a solid straight line in graphs. Fig. 9(a)-(b) shows the longitudinal bar strain through ascending drift ratio (first cycle at each drift ratio was considered) at different levels of the height of the column, where strain gauges were attached. It can be seen that in both FC and SC specimens, at about drift ratio of 1%, longitudinal reinforcements were yielded. SC specimen, which was suffered shear failure mode, longitudinal bar strains fluctuated in a wider range than FC specimen after

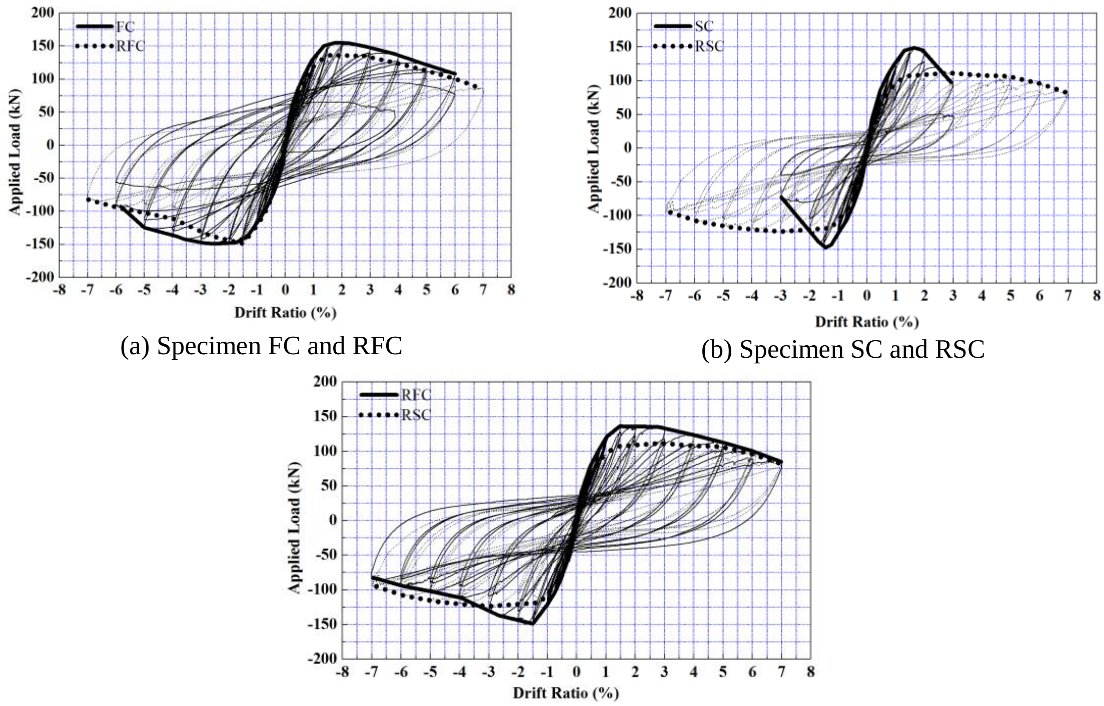

(a) Specimen FC and RFC

(b) Specimen SC and RSC

(c) Specimen RFC and RSC

Fig. 10 Load-drift envelope curves of the specimens in comparison yielding. Significant difference in transverse bar strain can be found between two specimens. In SC specimen in Fig. 9(b), at drift ratio of 3%, transverse bar strain reached the yield point while transverse reinforcements of FC specimen still behaved elastic until failure at 6% drift ratio. Maximum transverse strain observed in FC and SC specimen are 0.0009 and 0.0025, respectively.

Hysteretic curves of the specimens were also set for comparison with enveloped curves in Fig. 10. Figs. 10(a)-(b) show the effects of the SRF sheets and aramid rods in enhancing the ductility of the FC and SC specimens. In particular, RSC specimen performed a stable behavior, with a clear plateau after yielding, while its original SC specimen followed a sharp incline to failure. Fig. 10(c) illustrates the differences in the retrofitted specimens. The RFC specimens had superior strength as well as initial stiffness relative to the RSC specimen. However, due to the more stable behavior of RSC specimen after yielding and adopted method to calculate the ductility of the columns, it exceeded RFC specimens in terms of calculated ductility.

3.2 Energy dissipation of specimens

Energy dissipation, which is one of the fundamental indices used in evaluating the column's seismic response, was calculated in terms of energy dissipation per cycle and cumulative dissipated energy.

It is noted that energy dissipation is taken as the area enclosed by the corresponding load-displacement hysteretic curves. Table 6 and Fig. 11 present the value of energy dissipation for

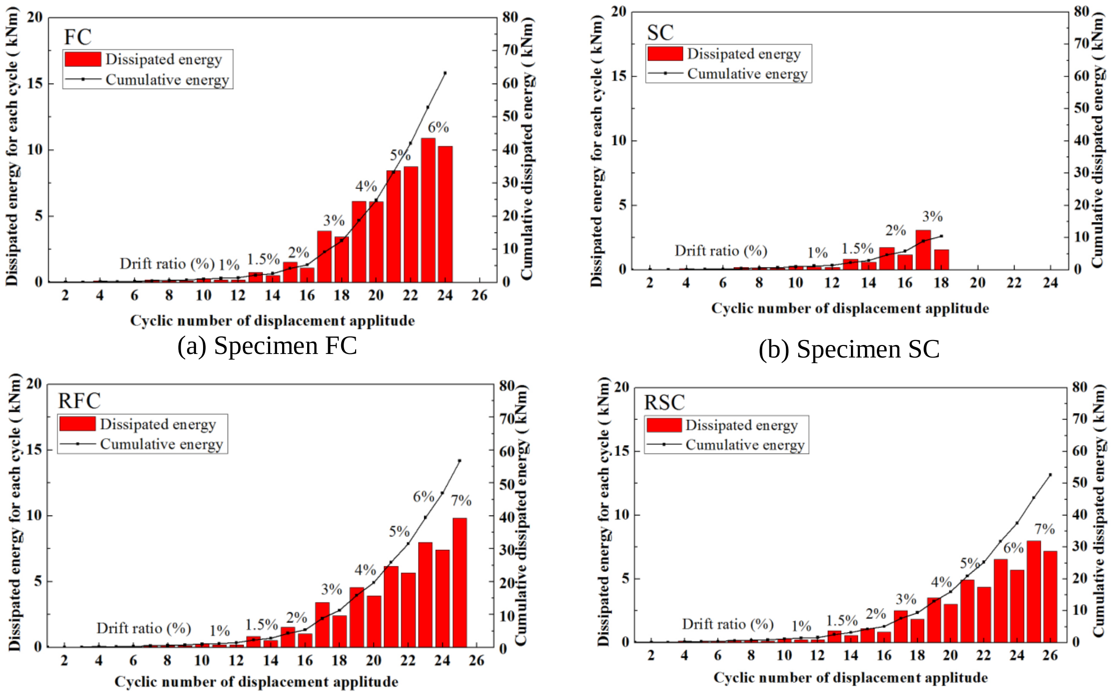

(a) Specimen FC (b) Specimen SC

(c) Specimen RFC (d) Specimen RSC

Fig. 11 Energy dissipation of the specimens

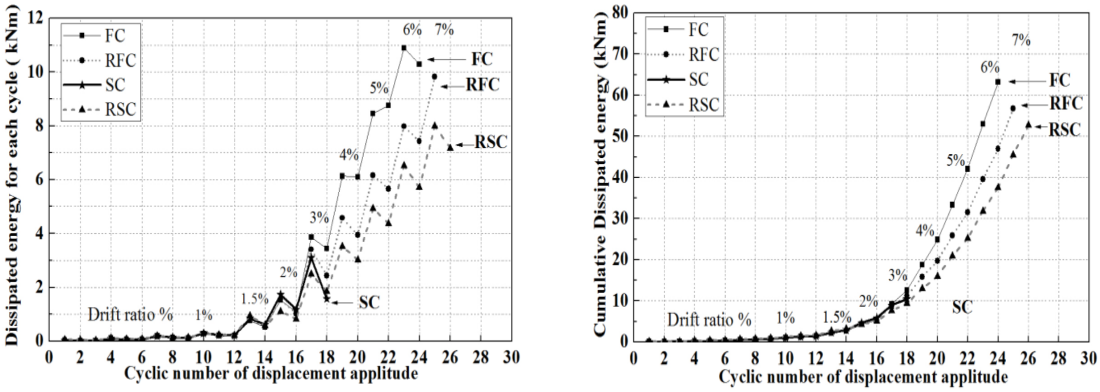

(a) Energy dissipation per cycle (b) Cumulative energy dissipation

Fig. 12 Energy dissipation of the specimens in comparison

Table 6 Measured energy dissipation of the specimens

Cycles	Drift ratio	Energy dissipation per cycle (kNm)			
		FC	RFC	SC	RSC
1		**0.04**	**0.12**	**0.03**	**0.24**
2	0.25%	0.02	0.04	0.02	0.12
3		0.01	0.08	0.01	0.12
4		**0.11**	**0.4**	**0.10**	**0.48**
5	0.50%	0.06	0.28	0.06	0.32
6		0.05	0.28	0.05	0.32
7		**0.19**	**0.64**	**0.19**	**0.8**
8	0.75%	0.13	0.52	0.14	0.56
9		0.11	0.48	0.12	0.48
10		**0.28**	**1.08**	**0.30**	**1.16**
11	1.0%	0.21	0.8	0.23	0.92
12		0.19	0.8	0.21	0.88
13	1.50%	**0.76**	**3.28**	**0.84**	**3.76**
14		0.52	2.16	0.61	2.28
15	2.0%	**1.53**	**6.2**	**1.73**	**4.44**
16		1.09	4.08	1.18	3.24
17	3.0%	**3.87**	**13.6**	**3.10**	**9.96**
18		3.44	9.68	1.57	7.32
19	4.0%	**6.13**	**18.28**		**14.08**
20		6.10	15.72		12.08
21	5.0%	**8.46**	**24.6**		**19.68**
22		8.75	22.6		17.44
23	6.0%	**10.89**	**31.88**		**26.08**
24		10.29	29.68		22.8
25	7.0%		**39.28**		**31.96**
26					28.64
Cumulative energy (kNm)		**63.26**	**56.76**	**10.5**	**52.64**

each specimen. Energy dissipation per cycle and cumulative energy dissipation of all specimens were compared in Fig. 12.

All specimens exhibited increasing energy dissipation per cycle through increasing drift ratios. It is noted that at each drift ratio from 0.25% to 1%, 3 cycles were repeated, and thereafter only 2 cycles were repeated for each drift ratio, from 1.5% up to the failure. It can be seen that all specimens exhibited the similar amount of energy dissipation per cycle from the beginning to 1.5% drift ratio. The discernible differences occurred at drift ratio of 2%, and with the failure of Specimen SC at 3% drift ratio, the FC specimen dissipated more energy per cycle than the RFS and RSC specimen. Though the FC specimen failed at 6% drift ratio, its energy dissipated per cycle still larger than that of the RFC and RSC specimens at 7% drift ratio.

The value of cumulative dissipated energy progressed in the following order: SC, RSC, RFC, FC specimen. The RFC specimen had lower energy dissipation than its primary specimens (56.76 kNm and 63.26 kNm respectively). Therefore, it may be said that SRF material and aramid rods had less effect on improving the energy-dissipating capacity of the flexural column specimens. In contrast, the RSC specimens exhibited more than 5 times energy dissipation than the SC specimen (52.64 kNm and 10.5 kNm). The similar amount of cumulative energy dissipation for the RFC and RSC strongly confirmed that the retrofitting material has extensively strengthened a shear specimen into a flexural-behaved specimen. However, the RFC specimen, which had aramid fiber rods, restored more column strength and initial stiffness that resulting in exhibiting higher energy than the RSC specimen.

4. Analytical modeling of the test specimens

The primary specimens of this experiment, FC and SC specimens, were analytically modeled using Zeus-NL, an analysis package of the Mid-American Earthquake Center. Taking account for shear deformation, column specimen was modeled with a shear spring (after Lee and Elnashai 2001) in parallel with the inelastic column element. The primary quatrilinear symmetric curve of the shear spring comprised of cracking, yielding and ultimate states, which were calculated utilizing the program Response 2000 (Bentz 2000). Fig. 13 presents the shear spring curve which was adopted for the modeling procedure. The hysteretic curves of the FC and SC specimens, which were obtained by using Response 2000 and that obtained by using Zeus-NL program without shear spring, were compared to define the primary curves. Concrete material was modeled based on the model of Kent and Park (1971) and reinforcement material was modeled using a bilinear elasto-plastic model with kinematic strain hardening.

Fig. 14 presents the stress-strain relationship of concrete and reinforcement that used for the modeling. Both confined and unconfined concrete model were adopted from Kent and Park (1971) proposal. Table 7 presents the formulas for calculating the ascending and the post-peak branch of the unconfined and confined concrete models in Fig 14(a). It is noted that, confinement only affected the slope of the post-peak branch. In this model, it is also assumed that concrete can sustain a stress of $0.2f_c'$ from a strain of ε_{20u} to infinite strain. Table 8, 9 and 10 present detailed values for the parameter adopted in the concrete, steel reinforcement and shear spring model.

Fig. 15 shows a comparison of the hysteretic curves of the column specimens between the experimental results (solid line) and the analytical results (dashed line). For the FC specimen, the

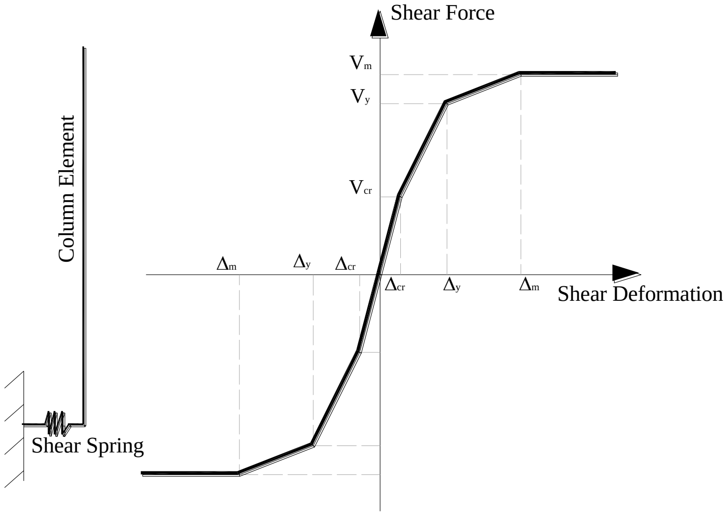

Fig. 13 Shear spring modeling in Zeus-NL (Elnashai 2004)

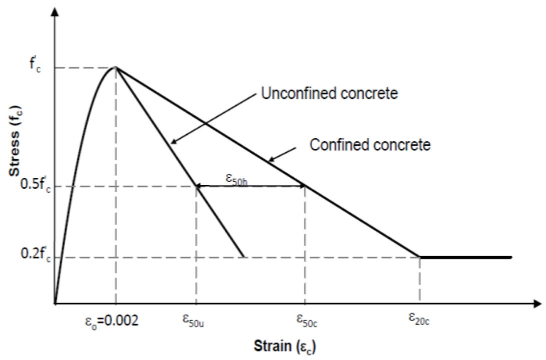

(a) Concrete model (Kent and Park 1971)

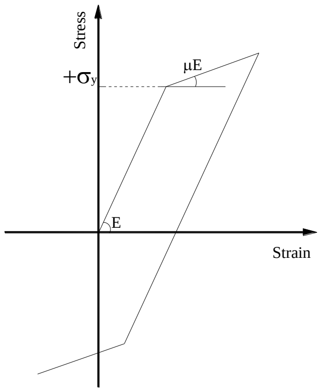

(b) Steel reinforcement model

Fig. 14 Stress-strain relationships used for modeling the materials

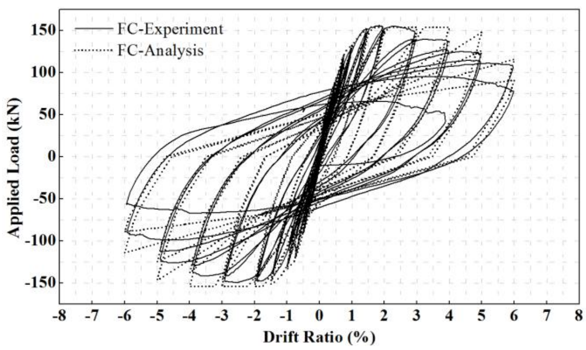

(a) Specimen FC

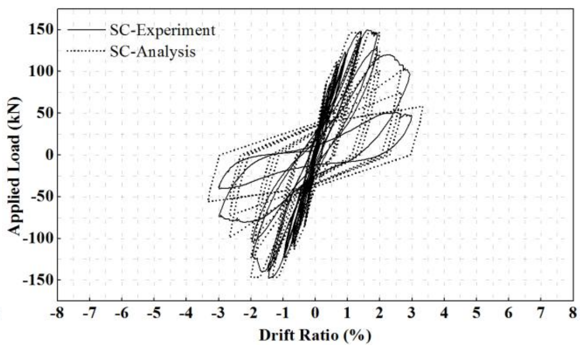

(b) Specimen SC

Fig. 15 Comparison between experimental and analytical results

Table 7 Concrete model formulas from Kent and Park (1971) proposal

Concrete model	Ascending branch	Post-peak branch
Unconfined	$f_c = f_c'\left[\frac{2\varepsilon_c}{0.002} - \left(\frac{\varepsilon_c}{0.002}\right)^2\right]$	$f_c = f_c'[1 - Z(\varepsilon_c - 0.002)]$ $Z = \frac{0.5}{\varepsilon_{50u} - 0.002}$ $\varepsilon_{50u} = \frac{3+0.29f_c'}{145f_c' - 1000}$ (f_c' in MPa)
Confined		$f_c = f_c'[1 - Z(\varepsilon_c - 0.002)]$ $Z = \frac{0.5}{\varepsilon_{50h} - \varepsilon_{50u} - 0.002}$ $\varepsilon_{50h} = \varepsilon_{50c} - \varepsilon_{50u} = \frac{3}{4}\rho''\sqrt{\frac{b''}{s}}$ $\varepsilon_{50u} = \frac{3+0.29f_c'}{145f_c' - 1000}$ (f_c' in MPa) $\rho'' = \frac{2(b''+d'')A_s''}{b''d''s}$

ε_{50u} : strain corresponding to the stress equal to 50% concrete maximum strength for unconfined concrete
ε_{50c} : strain corresponding to the stress equal to 50% concrete maximum strength for confined concrete
ρ'' : volumetric ratio of confining hoop to volume of concrete core measured to the outside of perimeter hoop
b'' : width of the confined core
d'' : depth of the confined core
$A''s$: cross-sectional area of the hoop bar
s: center to center spacing of the hoop

Table 8 Values for parameters in the concrete model (Unit: Mpa)

	Unconfined concrete model	Confined concrete model
Initial stiffness K_1	30,970	
Compressive strength	32.6	
Degradation stiffness K_2	-12150	-1581
Residual strength	6.52	

Table 9 Values for parameters in the steel reinforcement model (Unit: MPa)

	Steel reinforcement model
Young modulus E	190,870
Yield strength	484.7
Strain hardening μ	0.02

Table 10 Values for parameters in the shear spring model

Shear spring model parameters	FC specimen	SC specimen
Shear force at crack V_{cr} (kN)	69.3	38.5
Shear displacement at crack Δ_{cr} (mm)	0.56	0.17
Shear force at yielding V_y (kN)	123.2	84.7
Shear displacement at yielding Δ_y (mm)	2.56	0.83
Shear force at ultimate V_m (kN)	146.3	146.3
Shear displacement at ultimate Δ_m (mm)	6.69	5.41

maximum strength corresponding to the drift ratio of 4% and 5% was somewhat over estimated as the nonlinear behavior increased. For the SC specimen, the analytical model evaluated the seismic performance in terms of maximum strength as well as strength reduction as the inelastic deformation increased. Generally, all of the analytical models of the FC and SC specimens showed a good agreement in terms of maximum strength, initial stiffness and strength degradation at each loading step.

5. Conclusions

This research investigated the retrofitting of damaged RC column specimens, which were originally constructed to have certain flexural and critical failure mechanisms, with SRF and aramid fiber rods. The respective effect of each retrofitting method for each specimen can be summarized as follow.

SRF material significantly enhanced both the FC and SC column specimens in terms of ductility, stiffness degradation and energy dissipating capacity to prevent specimens from brittle failure. Especially, the RSC specimen, which previously experienced sudden brittle shear failure due to the poor confinement of transverse reinforcements, experienced a stable flexural behavior with ductility increased by 171%. However, in case of the RFC specimen, the effect was less significant than RSC specimen since only 18% of ductility increased. The level of effect seemed to depend on the failure mechanism of the original column specimen. The more brittle original column specimen behaved, the more significant retrofit effect was enhanced by the SRF materials.

Aramid fiber rods were also observed to enhance the strength of the column specimen. Extra aramid fiber rods improved load-bearing flexural capacity of the RFC specimen. Though neither of the RFC and RSC column specimens could sustained the same maximum load in the original columns, the RFC, which had extra aramid fiber rods, restored 88.4% of the maximum load while RSC specimen without the aramid rod only restored 74.5%.

Acknowledgments

This work was supported by the NRF (2012R1A2A2A06045129) & KAIA (13AUDP-B066083-01). The authors would like to express sincere gratitude for their support.

References

ACI (2011), *Building code requirements for structural concrete (ACI 318-11) and commentary* (ACI 318R-11), American Concrete Institute.

Aboutaha, R.S., Engelhardt, M.D., Jirsa, J.O. and Kreger, M.E. (1994), "Seismic shear strengthening of RC columns using rectangular steel jackets", *Fifth U.S National Conference on Earthquake Engineering*, July, Chicago, Illinois, 799-808.

Bayrak, O., Lacobucci, R.D. and Sheikh, S.A. (2003), "Retrofit of square concrete with carbon fiber-reinforced polymer for seismic resistance", *ACI Struct. J.*, **100**(6), 785-794.

Chang, C., Kim, S.J., Park, D. and Choi, S. (2014), "Experimental investigation of reinforced concrete columns retrofitted with polyester sheet", *Earthq. Struct.*, **6**(3), 237-250.

Choi, S.W., Kim, Y. and Park, H.S. (2014), "Multi-objective seismic retrofit method for using FRP jackets in shear-critical reinforced concrete frames", *Compos Part B.*, **56**, 207-216.

Colomb, F., Tobbi, H., Ferrier, E. and Hamelin, P. (2008), "Seismic retrofit of reinforced concrete short columns by CFRP materials", *Compos. Struct.*, **82**, 475-487.

Dai, J.G., Lam, L. and Ueda, T. (2012), "Seismic retrofit of square RC columns with polyethylene terephthalate (PET) fibre reinforced polymer composites", *Construct. Build Mater.*, **27**, 206-217.

Elnashai, A.S., Papanikolaou, V. and Lee, D. (2004), "Zeus NL - a system for inelastic analysis of structures", *Mid-America Earthquake Center CD-Release 04*, University of Illinois at Urbana-Champaign.

Ghobarah, A. and Galal, K.E. (2004), "Seismic rehabilitation of short rectangular RC columns", *J. Earthq. Eng.*, **8**(1), 45-68.

Han, S.W. and Jee, N.Y. (2005). "Seismic behaviors of columns in ordinary and intermediate moment resisting concrete frames", *Eng. Struct.*, **27**, 951-962.

Haroun, M.A. and Elsanadedy, H.M., (2005), "Behavior of Cyclically Loaded Squat Reinforced Concrete Bridge Columns Upgraded with Advanced Composite-Material Jackets", *J. Bridge Eng., ASCE*, November – December, 741-748.

Kabeyasawa, T., Tasai, A. and Igarashi, S. (2002), "An economical and efficient method of strengthening reinforced concrete columns against axial load collapse during major earthquake", *The Third Workshop on Performance-based Engineering on Reinforced Concrete Building Structures, Seattle*, WA. PEER Report 2002/02, 371-384

Kabeyasawa, T., Tasai, A. and Igarashi, S. (2004), "Test and analysis of reinforced concrete columns strengthened with polyester sheet", *Proceedings of 13th World Conference on Earthquake Engineering*, Vancouver, B.C., Canada, August.

Kim, Y., Kabeyasawa, T. and Igarashi, S. (2012), "Dynamic collapse test on eccentric reinforced concrete structures with and without seismic retrofit", *Eng. Struct.*, **34**, 95-110.

Le, T.K., Lee, K., Lee, J., Lee, D. and Woo, S. (2010), "Experimental study of RC beam-column joints strengthened using CFRP composites", *Compos. Part B.*, 134(8), 1288-1299.

Le, T.K., Lee, K., Shin, M. and Lee, J. (2011), "Analytical assessment and modeling of RC beam-column connections strengthened with CFRP composites", *Compos. Part B.*, **42**, 1786-1798.

Lee, D.H. and Elnashai, A.S. (2001), "Seismic analysis of RC bridge columns with flexure-shear interaction", *J. Struct. Eng.*, **127**(5), 546-553.

Meshaly, M.E., Youssef, M.A. and Elfath, H.M.A. (2014), "Use of SMA bars to enhance the seismic performance of SMA braced RC frames", *Earthq. Struct.*, **6**(3), 267-280.

Ozcan, O., Binici, B. and Ozcebe, G. (2008), "Improving seismic performance of deficient reinforced concrete piers using carbon fiber-reinforced polymers", *Eng Struct.*, **30**, 1632-1646.

Park, R. (1989), "Evaluation of ductility of structures and structural assemblages from laboratory testing", *Bulletin of the New Zealand National Society for Earthquakes Engineering*, **22**(3), 155-166.

Priestley, M.J.N., Verma, R. and Xiao, Y. (1994), "Seismic shear strength of reinforced concrete columns", *J. Struct. Eng. - ASCE*, 120(8), 2310-2329.

Priestley, M.J.N., Seible, F., Xiao, Y. and Verma, R. (1994), "Steel jacket retrofitting concrete bridge

columns for enhanced shear strength-part 2: Test results and comparison with theory", *ACI Struct. J.*, **91**(5), 537-551.
Sause, R., Harrries K.A., Walkup, S.L., Pessiki, S. and Ricles, J.M. (2004), "Flexural behavior of concrete piers retrofitted with carbon fiber-reinforced polymer jackets", *ACI Struct. J.*, 101-S70:708-716.
Seible, F., Priestley, M.J.N., Hegemier, G.A. and Innamorato, D. (1997), "Seismic retrofitting of RC with continuous carbon fiber jackets", *J. Compos. Construct.*, 52-62.
Sezen, H. and Chowdhury, T. (2009). "Hysteretic model for reinforced concrete columns including the effect of shear and axial load failure", *J Struct Eng, ASCE*, **135**(2), 139-146.
Sezen, H. and Moehle, J.P. (2006), "Seismic tests of concrete columns with light transverse reinforcement", *ACI Struct. J.*, **103**(6), 842-849.
Scott, B.D., Park, R. and Priestley, M.J.N. (1982), "Stress-strain behavior of concrete confined by overlapping hoops at low and high strain rates", *J. Am. Concrete Inst.*, **79**(1), 13-27.
Shin, M., Choi, Y., Kim, I. and Lee, K. (2013), "Effectiveness of low-cost fiber reinforced cement composites in hollow columns under cyclic loading", *Construct. Build. Mater.*, **47**, 623-635.